NUMERICAL SIMULATION OF THE EXTRUDATE-SWELL USING THE INTEGRAL KBKZ-PSM EQUATION

Juliana Bertoco, jubert@icmc.usp.br[1]
Murilo F. Tomé, murilo@icmc.usp.br[1]
[1]University of São Paulo, Av. Trabalhador São Carlense, 400, São Carlos, 13566590, Brazil

Abstract: *In this work is presented the numerical simulation of Extrudate-Swell problem using the integral KBKZ- PSM constitutive equation. The two-dimensional numerical method proposed herein is a finite difference technique for simulating flows possessing moving surfaces that can interact with solid walls. The momentum and mass conservation equations are solved by an implicit method. The integral equations describing the components of the extra-stress tensor are solved by a second-order quadrature formula and the Finger tensor is convected using the ideas of the deformation fields method proposed by Hulsen and co-workers. Integral constitutive models are known to provide a good fitting to the rheology of Boger fluids and polymer melts, as for example high density polyethylene (HDPE) and low density polyethylene (LDPE) that are usually employed by many industries. The results reported here were obtained using Boger Fluids. It is shown that the high elasticity effects exhibited by these solutions are well captured by the KBKZ-PSM integral model.*
Keywords: *KBKZ-PSM equations, Extrudate-Swell, Boger Fluids*

1. INTRODUCTION

Viscoelastic free surface flows are important in many industrial processes as for example in injection molding and profile extrusion. These problems are challenging as the flow may possess several moving free surfaces and although many researchers have been working on the development of numerical methods for simulating viscoelastic free surface flows, the accurate application of the free surface stress conditions is a problem that has not yet been fully tackled. Most of the works and methods to deal with free surface flows of viscoelastic fluids concern constitutive equations of differential type such as the well known models as UCM , Oldroyd-B and Phan-Thien-Tanner (see Tomé *et al.* (2012), Bonito *et al.* (2006), Tomé *et al.* (2010)), among others. Notwithstanding, the advances in computational resources have motivated researchers to consider more sophisticated rheological models that employ integral equations instead of partial differential equations. One reason is that integral constitutive models are known to provide a good approximation to the rheology of the fluid. One good example is the simulation of extrudate swell using Boger fluids of type M1. This fluid was initially simulated with the Oldroyd-B constitutive equations, which seemed to be appropriate due to its characteristics (see Mitsoulis (2010)). However the results compared well with the experiments only in regions of low shear rate. In this case, the results were uninteresting. The extrudate swell of several Boger fluids (e.g. M1, B, B2) were simulated by Mitsoulis (2010) who employed the KBKZ-PSM model to solve the governing equations using a finite element code. In this work, Mitsoulis says that in higher shear rate zones, the extrudate swell showed a tendency to abandon linear or quadratic behaviour and assumed a nonlinear one. This nonlinear behaviour was corrected captured by the KBKZ-PSM model. In the works of Chai and Yeow (1990), Trang and Yeow (2010), Mitsoulis (2010) and Tomé *et al.* (2016), the extrudate swell problem was solved and a high extrudate swell ratio was obtained.

We present a numerical method for solving two-dimensional flows governed by the K-BKZ/PSM integral constitutive equation that is capable of resolving multiple moving free surface flows and their interaction with rigid walls. We formulate an algorithm to resolve the governing equations and employ the finite difference method to solve the basic equations. The complex phenomenon of extrudate swell is studied for high shear flows of a Boger Fluid M1.

2. GOVERNING EQUATIONS

For isothermal incompressible flows, the mass conservation and the equation of motion in dimensionless form, can be written as (for details, see Tomé *et al.* (2008))

$$\nabla \cdot \mathbf{v} = 0 \,, \tag{1}$$

$$\frac{\partial \mathbf{v}}{\partial t} + \nabla \cdot (\mathbf{vv}) = -\nabla p + \frac{1}{Re}\nabla^2 \mathbf{v} + \nabla \cdot \mathbf{\Phi} + \frac{1}{Fr^2}\mathbf{g} \,. \tag{2}$$

The non-Newtonian tensor $\mathbf{\Phi}$ is related to the extra-stress tensor $\boldsymbol{\tau}$, through the following EVSS transformation

$$\mathbf{\Phi} = \boldsymbol{\tau} - \frac{1}{Re}\dot{\boldsymbol{\gamma}} \,, \text{ where } \dot{\boldsymbol{\gamma}} = \nabla \mathbf{v} + (\nabla \mathbf{v})^{\mathrm{T}}. \tag{3}$$

In this work, is adopted the KBKZ/PSM integral constitutive equation for defined the rheological behaviour of fluid flow (for details, see Mitsoulis (2013))

$$\boldsymbol{\tau}(t) = \int_{-\infty}^{t} M(t-t')H(I_1, I_2)\mathbf{B}_{t'}(t)dt' \,, \tag{4}$$

$$\text{where} \qquad M(t-t') = \sum_{k=1}^{m_1} \frac{a_k}{\lambda_k Wi} e^{-\frac{t-t'}{\lambda_k Wi}} \qquad \text{and} \qquad H(I_1, I_2) = \frac{\alpha}{\alpha - 3 + \beta I_1 + (1-\beta)I_2}. \tag{5}$$

In the memory function, λ_k, a_k, m_1 are relaxation times, relaxation modules and the number of relaxation modes, respectively. These parameters and α, β are obtained from a curve fitting to the rheological properties of the fluid. The function $H(I_1, I_2)$ is the Papanastasiou-Scriven-Macosko damping function (see Papanastasiou *et al.* (1983)) and $\mathbf{B}_{t'}(t)$ is the Finger tensor. The quantities I_1 and I_2 are the first and second invariants of $\mathbf{B}_{t'}(t)$, respectively.

In these equations, $Re = \dfrac{\rho_0 UL}{\eta_0}$ is the Reynolds number, $Fr = \dfrac{U}{\sqrt{L\,g}}$ is the Froude number and $Wi = \lambda_{ref}\dfrac{U}{L}$ is the Weissenberg number, where U and L are velocity and length scales and $g, \eta_0, \rho_0, \lambda_{ref}$ are the gravity acceleration, fluid viscosity, fluid density and a reference relaxation time, respectively.

The equations (1)-(5) are solved for two-dimensional Cartesian time-dependent flows where $\mathbf{v} = (u(x,y,t),\ v(x,y,t))^T$, $p = p(x,y,t)$,

$$\boldsymbol{\tau}(x,y,t) = \begin{bmatrix} \tau^{xx} & \tau^{xy} \\ \tau^{xy} & \tau^{yy} \end{bmatrix}, \quad \boldsymbol{\Phi}(x,y,t) = \begin{bmatrix} \Phi^{xx} & \Phi^{xy} \\ \Phi^{xy} & \Phi^{yy} \end{bmatrix}, \quad \text{and} \quad \mathbf{B}_{t'(t)}(x,y,t) = \begin{bmatrix} B^{xx} & B^{xy} & 0 \\ B^{xy} & B^{yy} & 0 \\ 0 & 0 & 1 \end{bmatrix}.$$

Note that to compute the stresses for 2D flows we need to consider the 3D Finger tensor as shown.

2.1 Boundary conditions

Appropriate boundary conditions for the velocity field must be specified to solve the equations (1)-(3). At fluid entries the velocity is prescribed while at fluid exits fully developed flow is assumed and so the homogeneous Neumann condition, is applied. On the fluid surfaces, we consider unsteady free surface flows of fluids moving into a passive atmosphere. In the absence of surface tension forces, the normal and tangential components of stress must be continuous across any surface, so (see Batchelor (1967))

$$\mathbf{n}\cdot\boldsymbol{\sigma}\cdot\mathbf{n}^{\mathrm{T}} = 0 \qquad \text{and} \qquad \mathbf{m}\cdot\boldsymbol{\sigma}\cdot\mathbf{n}^{\mathrm{T}} = 0\,, \tag{6}$$

where $\mathbf{n}$ is the unit outward normal vector to the free surface and $\mathbf{m}$ is the associated unit tangential vector. The total stress tensor, $\boldsymbol{\sigma}$ is given by

$$\boldsymbol{\sigma} = -p\mathbf{I} + \frac{1}{Re}\dot{\boldsymbol{\gamma}} + \boldsymbol{\Phi}\,, \tag{7}$$

where $\boldsymbol{\Phi}$ and $\dot{\boldsymbol{\gamma}}$ are the tensors obtained from the application of the EVSS transformation (3).

3. NUMERICAL METHOD

The governing equations are solved by a variant of the original Marker-And-Cell method that employs the finite difference method on a staggered grid. The velocity components are located at the middle of cell faces while the other variables, are positioned at cell centre.

The fluid surface is represented by marker particles that move with the local fluid velocity. Visualization of the fluid flow is provided by conecting these particles by straight lines and the volume of fluid is defined by the area of the closed curve defined by the corresponding pieciewise linear curve. For detais see Tomé *et al.* (2000).

The solutions $\mathbf{v}(\mathbf{x}, t_{n+1})$, $p(\mathbf{x}, t_{n+1})$ and $\boldsymbol{\tau}(\mathbf{x}, t_{n+1})$ at time $t_{n+1} = t + \delta t$ are obtained in two parts: first, using the values of $\boldsymbol{\tau}(\mathbf{x}, t)$, the velocity and pressure fields are calculated at time t_{n+1}. Then, $\mathbf{v}(\mathbf{x}, t_{n+1})$ is employed to compute the tensor $\boldsymbol{\tau}(\mathbf{x}, t_{n+1})$ by the *deformation fields method* (Hulsen *et al.* (2001)), as follows.

3.1 Calculation of $\mathbf{v}(\mathbf{x}, t_{n+1})$ and $p(\mathbf{x}, t_{n+1})$

The numerical method employed to solve (1)-(2) is based on the implicit algorithm proposed by Oishi *et al.* (2011). It is assumed that at time t the variables $\mathbf{v}(\mathbf{x}, t) = \mathbf{v}^{(n)}$, $p(\mathbf{x}, t) = p^{(n)}$, $\boldsymbol{\tau}(\mathbf{x}, t) = \boldsymbol{\tau}^{(n)}$ and the markers' positions $\mathbf{x}(t) = \mathbf{x}^{(n)}$, are known. Then, $\mathbf{v}(\mathbf{x}, t_{n+1})$, $p(\mathbf{x}, t_{n+1})$ and $\mathbf{x}(t_{n+1})$ are obtained from the steps:

1. Calculate $\dot{\boldsymbol{\gamma}}^{(n)} = \left[\nabla\mathbf{v}^{(n)} + (\nabla\mathbf{v}^{(n)})^{\mathrm{T}}\right]$ and from (3) obtain $\boldsymbol{\Phi} = \boldsymbol{\tau}^{(n)} - \dfrac{1}{Re}\dot{\boldsymbol{\gamma}}^{(n)}$.

2. Calculate an intermediate velocity field $\widetilde{\mathbf{v}}^{(n+1)}$ by implicit Euler discretization of

$$\frac{\widetilde{\mathbf{v}}^{(n+1)}}{\delta t} - \frac{1}{Re}\nabla^2\widetilde{\mathbf{v}}^{(n+1)} = \frac{\mathbf{v}^{(n)}}{\delta t} - \nabla\cdot(\mathbf{vv})^{(n)} - \nabla p^{(n)} + \nabla\cdot\boldsymbol{\Phi} + \frac{1}{Fr^2}\mathbf{g}, \tag{8}$$

3. Solve the Poisson equation for the potential function ψ:

$$\nabla^2\psi^{(n+1)} = \nabla\cdot\widetilde{\mathbf{v}}^{(n+1)}. \tag{9}$$

The boundary conditions required for solving this Poisson equation are the homogeneous Neumann conditions for rigid walls and inflows, while homogeneous Dirichlet conditions are applied at outflows. This equation is solved for every Full and Surface cell by using the formulation introduced by Oishi *et al.* (2011).

4. Compute the final velocity field from equation

$$\mathbf{v}^{(n+1)} = \widetilde{\mathbf{v}}^{(n+1)} - \nabla\psi^{(n+1)}. \tag{10}$$

5. Compute the final pressure field

$$p^{(n+1)} = p^{(n)} + \frac{\psi^{(n+1)}}{\delta t} - \frac{1}{Re}\nabla^2\psi^{(n+1)} \tag{11}$$

The equations in steps 1. to 5. are solved by a second-order finite difference technique. Details of the finite difference equations involved are given in Oishi *et al.* (2011) and for lack of space are not detailed here.

3.2 Calculation of the extra-stress tensor $\boldsymbol{\tau}(\mathbf{x}, t_{n+1})$

To calculate the extra-stress tensor $\boldsymbol{\tau}(\mathbf{x}, t_{n+1})$ we employ the methodology presented in Tomé *et al.* (2016) as follows. Let $t_j^{'}, j = 0, 1, \cdots, N$, be $(N+1)$-points in the interval $[0,\ t_{n+1}]$. Then the constitutive equation (4) can be written in the form

$$\begin{aligned}\boldsymbol{\tau}(t_{n+1}) = &\int_{-\infty}^{0} M(t_{n+1}-t^{'})H(I_1,I_2)\mathbf{B}_{t'}(t_{n+1})dt' \\ &+ \sum_{j=0}^{\frac{N-2}{2}}\int_{t_{2j}^{'}}^{t_{2j+2}^{'}} M(t_{n+1}-t')H(I_1,I_2)\mathbf{B}_{t'}(t_{n+1})dt'\ ,\end{aligned} \tag{12}$$

where N even is adopted. For $t^{'} < 0, \mathbf{B}_{t'}(t_{n+1}) = \mathbf{B}_0(t_{n+1})$ and therefore, the first integral becomes

$$\int_{-\infty}^{0} M(t_{n+1})H(I_1(\mathbf{B}_0(t_{n+1})), I_2(\mathbf{B}_0(t_{n+1})))\,\mathbf{B}_0(t_{n+1})dt' \tag{13}$$

and can be solved exactly. For the integrals under the summation operator in equation (12), the points $t_j^{'}$ are not equally spaced and a second-order quadrature formula is employed. Each integral $\int_{t_{2j}^{'}}^{t_{2j+2}^{'}} M(t_{n+1}-t')H(I_1,I_2)\mathbf{B}_{t'}(t_{n+1})dt'$ is approximated by the 3-node quadrature formula

$$\begin{aligned}I_3 = \ & A_0 * H(I_1(\mathbf{B}_{t_{2j}^{'}}(t_{n+1})), I_2(\mathbf{B}_{t_{2j}^{'}}(t_{n+1}))) * \mathbf{B}_{t_{2j}^{'}}(t_{n+1}) * M(t_{n+1}-t_{2j}^{'}) \\ &+ A_1 * H(I_1(\mathbf{B}_{t_{2j+1}^{'}}(t_{n+1})), I_2(\mathbf{B}_{t_{2j+1}^{'}}(t_{n+1}))) * \mathbf{B}_{t_{2j+1}^{'}}(t_{n+1}) * M(t_{n+1}-t_{2j+1}^{'}) \\ &+ A_2 * H(I_1(\mathbf{B}_{t_{2j+2}^{'}}(t_{n+1})), I_2(\mathbf{B}_{t_{2j+2}^{'}}(t_{n+1}))) * \mathbf{B}_{t_{2j+2}^{'}}(t_{n+1}) * M(t_{n+1}-t_{2j+2}^{'}).\end{aligned} \tag{14}$$

The coefficients A_0, A_1, A_2 are obtained by solving the (3×3)-linear system

$$A_0 + A_1 + A_2 = b_0 = \int_{t_{2j}}^{t_{2j+2}} dt^{'}, \tag{15}$$

$$A_0 * t_{2j}^{'} + A_1 * t_{2j+1}^{'} + A_2 * t_{2j+2}^{'} = b_1 = \int_{t_{2j}}^{t_{2j+2}} t^{'}\ dt^{'}, \tag{16}$$

$$A_0 * (t_{2j}^{'})^2 + A_1 * (t_{2j+1}^{'})^2 + A_2 * (t_{2j+2}^{'})^2 = b_2 = \int_{t_{2j}}^{t_{2j+2}} (t^{'})^2\ dt^{'}, \tag{17}$$

and are found to be

$$A_2 = \frac{t_{2j+1}t_{2j}b_0 + b_2 - t_{2j}b_1 - t_{2j+1}b_1}{t_{2j+2}^2 - t_{2j+1}t_{2j+2} + t_{2j+1}t_{2j} - t_{2j}t_{2j+2}}\ , \tag{18}$$

$$A_1 = \frac{-t_{2j}b_1 + t_{2j}b_0t_{2j+2} + b_2 - t_{2j+2}b_1}{(t_{2j+1}-t_{2j})(t_{2j+1}-t_{2j+2})}\ , \tag{19}$$

$$A_0 = -\frac{-t_{2j+1}b_1 + t_{2j+1}b_0t_{2j+2} + b_2 - t_{2j+2}b_1}{(-t_{2j+2}+t_{2j})(t_{2j+1}-t_{2j})}\ . \tag{20}$$

The points $t_j^{'}(t_{n+1})$ are obtained from a *geometric progression* as follows.

1. Set $t_0^{'} = 0$ and $t_N^{'} = t_{n+1}$;

2. $t_{N-j}^{'} = t_N^{'} - q^j,\ j = 1, 2, \cdots, N-1$, where $q = (t_{n+1}/\delta t)^{1/N}$, dt is the time-step employed for calculating the velocity and pressure.

The Finger tensor $\mathbf{B}_{t'(t)}(\mathbf{x}, t)$ is computed according to the *deformation fields method* (Hulsen *et al.* (2001)) and is computed by

$$\frac{\partial}{\partial t}\mathbf{B}_{t'(t)}(\mathbf{x}, t) + \mathbf{v}(\mathbf{x}, t) \cdot \nabla \mathbf{B}_{t'(t)}(\mathbf{x}, t) = [\nabla \mathbf{v}(\mathbf{x}, t)]^T \cdot \mathbf{B}_{t'(t)}(\mathbf{x}, t) + \mathbf{B}_{t'(t)}(\mathbf{x}, t) \cdot \nabla \mathbf{v}(\mathbf{x}, t)\ , \tag{21}$$

with the condition $\mathbf{B}_{t'=t_{n+1}}(\mathbf{x}, t_{n+1}) = \mathbf{I}$.
For details see Tomé *et al.* (2016)

4. VERIFICATION OF THE TECHNIQUE

The numerical technique described in Section 3 has been verified against an analytic solution for channel flows. Several increasing meshes were employed in the calculations and the results showed convergence of the numerical results. With regard to free surface flows, a numerical convergence verification was undertaken which showed a jet hitting a flat surface using varius meshes. Moreover, a numerical comparison of the simulation of a specific extrudate swell problem with those results of Mitsoulis (2010). All these verifications produced good results and are detailed in Tomé *et al.* (2016).

5. SIMULATION OF THE EXTRUDATE SWELL OF BOGER FLUID M1

The technique described in Section 3 was applied to simulate the extrudade swell of a Boger fluid M1. This fluid was originally characterized by Chai and Yeow (1990) and posteriorly modified by Mitsoulis (2010). Its spectrum contains 3 relaxation times which are given in Tab. 1.
To simulate this problem, the flow domain used is depicted in Fig. 1 in which the yellow and pink regions denote an inflow and outflow boundaries, respectively.

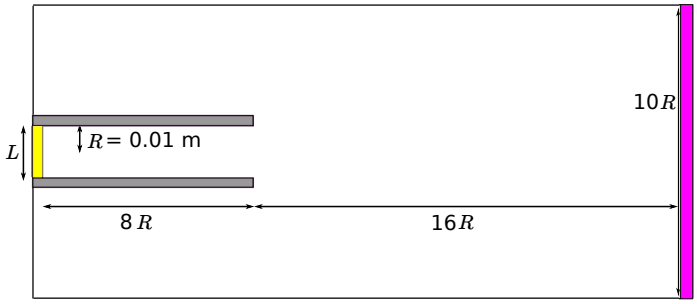

Figure 1: **Description of the domain used in the simulation of the extrudate swell**.

Table 1: **Data defining fluid M1 (from Mitsoulis (2010))**.

Fluid M1		
$\rho_0 = 868\,kg/m^3$, $\eta_0 = 2.4$ Pa.s		
$\alpha = 34214$, $\beta = 0.1$, $\lambda_{ref} = 0.081$s		
k	λ_k	a_k
1	4.887×10^{-4}s	3129.5Pa
2	4.464×10^{-2}s	5.0917Pa
3	2.8384×10^{-1}s	2.2783Pa

The simulations presented here were performed for several values of the *apparent shear rate*, $\dot{\gamma}_a$, which is defined in terms of the volumetric rate Q and the width L of the channel (see Mitsoulis (2010)) by $\dot{\gamma}_a = 3U/L$, where U is a characteristic velocity. By using the data displayed in Tab. 2, a total of five simulations were carried out. A mesh with $\delta x = \delta y = L/16$ was employed in these simulations.

Table 2: **Input data used in the simulations.**

$\dot{\gamma}_a\,(s^{-1})$	$U\,(ms^{-1})$	Re	Wi
12	0.080	0.57	0.32
13	0.086	0.62	0.35
14	0.093	0.67	0.37
15	0.100	0.72	0.40
16	0.106	0.77	0.43

The viscoelasticity of the fluid was measured in terms of the stress ratio, S_R, given by (see Tanner (2000))

$$S_R = \frac{N_{1,w}}{2\tau_{,w}^{xy}} = \frac{\left(\tau^{xx} - \tau^{yy}\right)_{,w}}{2\tau_{,w}^{xy}},\ \text{where } N_{1,w} \text{ and } \tau_{,w}^{xy} \text{ were evaluated at the die wall, before the channel exit.}$$

At the fluid entrance (inflow) the velocity was given by a parabolic profile having maximum velocity U and the Finger tensor components were defined by the exact solution of shear flow (see Tomé *et al.* (2016)) while at the outflow, both the velocity and the Finger tensor obeyed homogeneous Neumann conditions.

The simulations started with an empty channel and the fluid was injected in throughout the channel entrance until it flowed out the channel exit and extruded into the air where the stresses were relaxed making the fluid to swell. All the simulations were performed until $t = 20$s. Fig. 2 displays several snapshots of the fluid configuration, for $\dot{\gamma}_a = 16$, at different times showing the development of the fluid free surface inside and outside the channel. At time $t = 20$s we can see that the fluid already reached the outflow boundary and the fluid surface is smooth displaying no changes. We expect that at this time, steady state flow has been stablished.

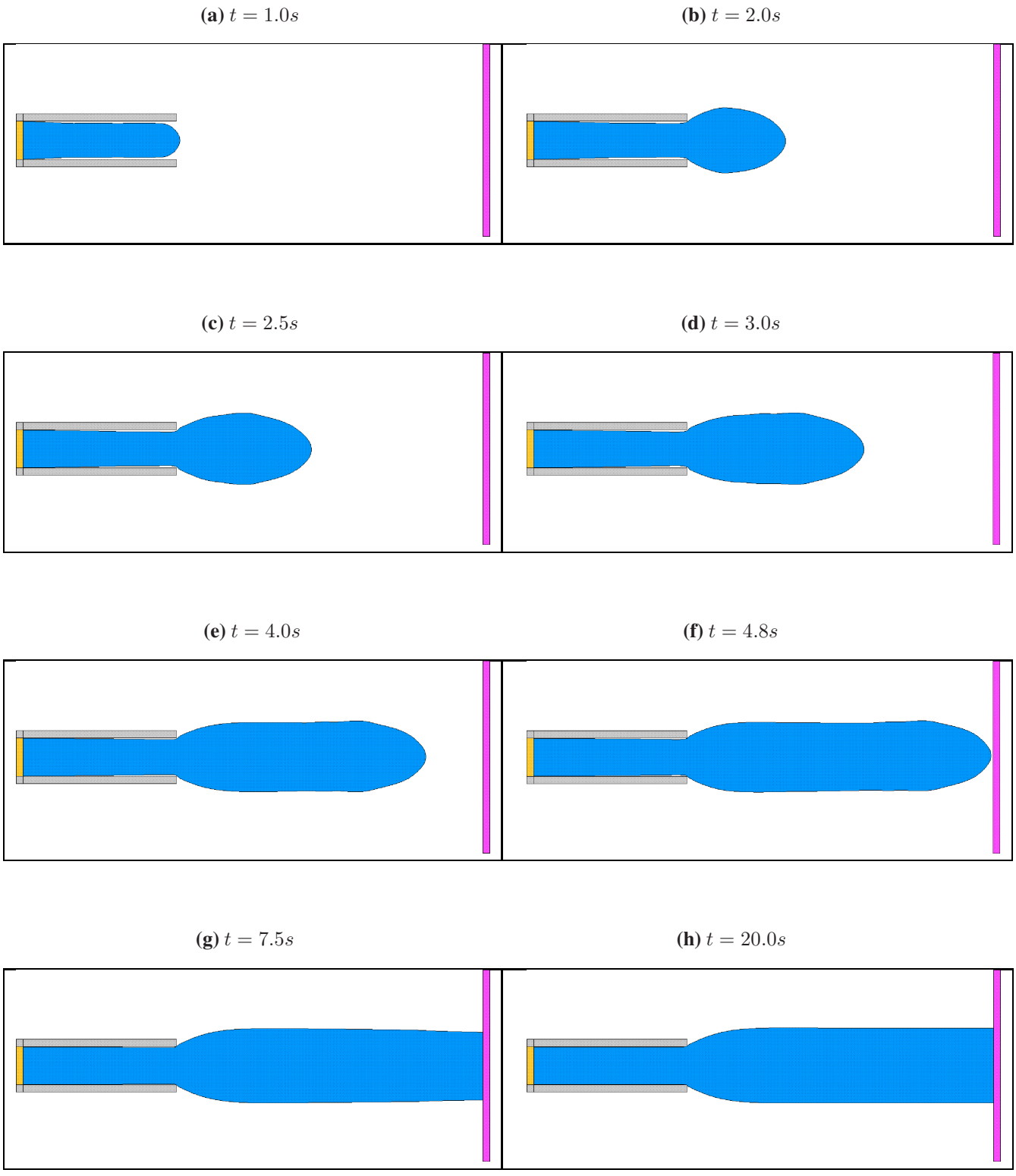

Figure 2: **Fluid flow visualization at several times. Results obtained with** $Re = 0.77, Wi = 0.43, \dot{\gamma}_a = 16$.

Figure 3 displays the extrudate ratios $\chi = D_{max}/L$, where D_{max} is the maximum swell, obtained in all simulations while Tab. 3 presents the stress ratios S_R and χ. For comparison, the results obtained by Mitsoulis (2010) with $Re = 0$ and $\dot{\gamma}_a = 12, 15$ are also shown. The results displayed in Tab. 3 show that high swelling ratios, up to 100%, were attained indicating that the numerical technique presented in this work is capable of dealing with high elastic fluids. Moreover, it is shown that our results agree well with Mitsoulis's predictions for χ with $\dot{\gamma}_a = 12$ and 15.

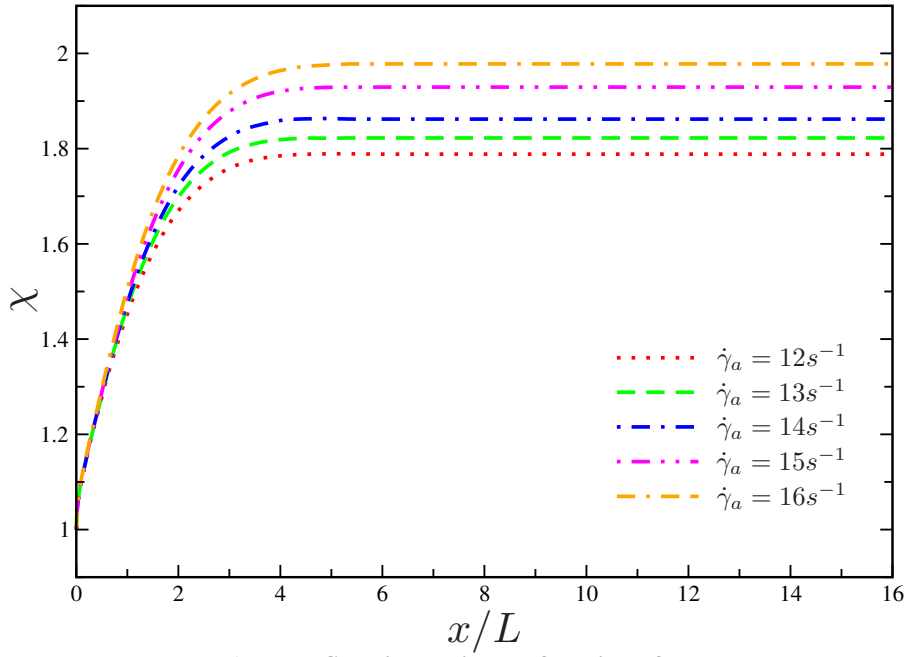

Figure 3: **Swelling ratio as a function of $\dot{\gamma}_a$.**

Table 3: **Results obtained in the simulation of the extrudade swell.**

$\dot{\gamma}_a\,(s^{-1})$	This Work - SR	Mitsoulis - SR	This Work - χ	Mitsoulis - χ
12	1.14	0.97	1.79	1.76
13	1.24	−−	1.82	−−
14	1.33	−−	1.88	−−
15	1.43	1.21	1.92	1.94
16	1.53	−−	1.96	−−

6. CONCLUDING REMARKS

This work presented a numerical technique for solving viscoelastic flows governed by the integral constitutive equation K-BKZ PSM. Verification results in channel flow and free surface flows were obtained which showed convervenge with mesh refinement (see Tomé *et al.* (2016)). This technique was applied to simulate the extrudate swell of a fluid M1 for various values of the *apparent shear rate*, $\dot{\gamma}_a$. The results displayed high extrudate ratios indicating that our method can cope with high elastic fluids modeled by the K-BKZ PSM integral equation. Moreover, the results with $\dot{\gamma}_a = 12$ and 15 were compared with those of Mitsoulis and good agreement was obtained. In summary, this technique demonstrated capable of dealing with the extrudate swell problem of fluid M1.

7. ACKNOWLEDGEMENTS

The authors acknowledge the financial support given by the funding agencies: CAPES (Coordenação de Aperfeiçoamento de Pessoal de Nível Superior) - Grants Nos. DO/5633919 and PDSE-99999.003603/2014-08 ; Cnpq (Conselho Nacional de Desenvolvimento Científico e Tecnológico) - Grants Nos. 306280/2014-0; FAPESP (Fundação de Amparo a Pesquisa do Estado de São Paulo) - Grants Nos. 2014/21415-7 and 2013/07375-0 (CEPID-CeMEAI project).

8. REFERENCES

Batchelor, G.K., 1967. *An Introduction of Fluid Dynamics*. Cambridge University Press, Cambridge.

Bonito, A., Picasso, M. and Laso, M., 2006. "Numerical simulation of 3d viscoelastic flows with free surfaces". *J. of Computational Physics*, No. 215, pp. 691–716.

Chai, M.S. and Yeow, Y.L., 1990. "Modelling of fluid m1 using multiple-relaxation-time constitutive equations". *J. of Non-Newtonian Fluid Mechanics*, No. 35, pp. 459–470.

Hulsen, M.A., Peters, E.A.J.F. and van den Brule, B.H.A.A., 2001. "A new approach to the deformation fields method for solving complex flows using integral constitutive equations". *J. of Non-Newtonian Fluid Mechanics*, No. 98, pp. 201–221.

Mitsoulis, E., 2010. "Extrudate swell of boger fluids". *J. of Non-Newtonian Fluid Mechanics*, No. 165, pp. 812–824.

Mitsoulis, E., 2013. "50 years of the k-bkz constitutive relation for polymers". *Polymer Science*.

Oishi, C.M., Martins, F.P., Tomé, M.F., Cuminato, J.A. and McKee, S., 2011. "Numerical solution of the extended pom-pom model for viscoelastic free surface flows". *J. of Non-Newtonian Fluid Mechanics*, No. 166, pp. 165–179.

Papanastasiou, A.C., Scriven, L.E. and Macosko, C.W., 1983. "An integral constitutive equation for mixed flows: viscoelastic characterization". *J. of Rheology*, No. 27, p. 387.

Tanner, R.I., 2000. *Engineering Rheology*. Oxford University Press, Oxford.

Tomé, M.F., Araujo, M.S.B., Alves, M.A. and Pinho, F.T., 2008. "Numerical simulation of viscoelastic flows using integral constitutive equations: a finite difference approach". *J. of Computational Physics*, No. 227, pp. 4207–4243.

Tomé, M.F., Bertoco, J., Oishi, C.M., Araujo, M.S.B., Cruz, D., Pinho, F.T. and Vynnycky, M., 2016. "A finite difference technique for solving a time strain separable k-bkz constitutive equation for two-dimensional moving free surface flows". *J. of Computational Physics*, No. 311, pp. 114–141.

Tomé, M.F., Castelo, A., Afonso, A.M., Alves, M.M. and Pinho, F.T., 2012. "Application of the log-conformation tensor to three-dimensional time-dependent free surface flows". *J. of Non-Newtonian Fluid Mechanics*, No. 175-176, pp. 44–54.

Tomé, M.F., Cuminato, J.A., Cesar, C.N.L. and McKee, S., 2000. "Freeflow: an integrated simulation system for three-dimensional free surface flows". *Computing and Visualization in Science*, No. 2, pp. 199–219.

Tomé, M.F., Paulo, G.S., Alves, M.A. and Pinho, F.T., 2010. "Numerical solution of the ptt constitutive equation for three-dimensional free surface flows". *J. of Non-Newtonian Fluid Mechanics*, No. 165, pp. 247–262.

Trang, C.T. and Yeow, Y.L., 2010. "Extrudate swell of newtonian and non-newtonian fluids—the effect of gravitational body force". *J. of Non-Newtonian Fluid Mechanics*, No. 20, pp. 103–116.